AIP | Journal of Applied Physics

# Study of laser excited vibration of silicon cantilever

Yaqin Song, Bernard Cretin, D. M. Todorović, and Pascal Vairac

Citation: Journal of Applied Physics **104**, 104909 (2008); doi: 10.1063/1.2987470
View online: http://dx.doi.org/10.1063/1.2987470
View Table of Contents: http://scitation.aip.org/content/aip/journal/jap/104/10?ver=pdfcov
Published by the AIP Publishing

# Study of laser excited vibration of silicon cantilever

Yaqin Song,[1,2] Bernard Cretin,[1,a)] D. M. Todorović,[3] and Pascal Vairac[1]
[1]*FEMTO-ST Institute, Université de Franche-Comté–CNRS–ENSMM–UTBM, 32, Avenue de l'Observatoire, 25044 Besançon Cedex, France*
[2]*MOE Key Laboratory for Strength and Vibration, School of Aerospace, Xi'an Jiaotong University, 710049 Xi'an, People's Republic of China*
[3]*Center for Multidisciplinary Studies, University of Belgrade, Kneza Viseslava, 11030 Belgrade, Serbia*

(Received 18 March 2008; accepted 5 August 2008; published online 20 November 2008)

In this paper an interferometric setup called "thermoelastic microscopy" has been used to measure the vibration response of the semiconductor cantilevers under modulated laser thermal source. The small vibration amplitude has been detected well below 10 pm magnitude in accurate adjustment conditions. The results showed that experimental responses have a good agreement with the theoretical ones. Also from the analysis we could conclude that the signal amplitude has a power functional dependence on the modulation frequency and that the phase angle linearly depended on the square root of modulation frequency. © *2008 American Institute of Physics*.
[DOI: 10.1063/1.2987470]

## I. INTRODUCTION

The development of microsystem (nanosystem) technologies (surface and bulk micromachining) resulted in the production of miniature sensors, actuators, resonators, and electromechanical parts. Cantilever is one kind of highly sensitive sensor and has received a great deal of attention in physical, chemical, biological, and mechanical systems. This is primarily due to its high sensitivity, flexibility, and reliability. These characterizations enable us to detect small changes in properties, either as a change of deflection or of resonance frequency.[1] Usually the resonant frequency and $Q$-factor of vibrated cantilever are output parameters of this kind of sensors. They are sensitive to external parameters such as force, pressure, temperature, or medium viscosity and density. During the past ten years, many publications devoted to study of the cantilever sensors experimentally and theoretically, especially for microscale cantilever sensors. In this paper we are interested in millimeter-sized cantilevers. Until now, there are many works on this topic.[2–5] But to our knowledge, many of these works focused on the application of cantilever to detect the change in resonance frequency induced by piezoelectric excited under different surrounding media (gases or liquids). However, as is well known there are always some problems for piezoelectric materials, such residual deformation and residual stress, they will severely affect the sensitivity and repeatability of the sensors.

So far the photoacoustic (PA) and photothermal (PT) science and technology have extensively developed new methods of investigation of semiconductors and microelectronic structures.[6–11] Due to the merits of noncontact and nondestructive behavior, these methods are widely used as a detection way in microelectromechanical system (MEMS) and nanoelectromechanical system, especially in situations where other techniques are not useful.[12] They can be used to reveal surface and subsurface structure of samples and also to obtain the material properties such as thermal conductivity, thermal diffusivity, etc. A lot of excellent works have been done both in experimental and in theoretical fields.[13–21]

For semiconductor materials plasma waves, generated by the absorbed intensity-modulated laser beam, can play the dominant role in the PA and PT experiments. Depth-dependent plasma waves contribute to the generation of periodic heat and mechanical vibrations, i.e., thermoelastic (TE) deformation. Also the photoexcited carriers produce periodic elastic deformation, i.e., electronic deformation (ED), in the sample. TE and ED are prominent deformations of semiconductor samples under PA and PT effects.[22] Absorption of the modulated optical energy in a semiconducting cantilever causes various TE and ED effects. The TE and ED effects can be important as driven mechanisms for micromechanical structures, especially for cantilevers.[22] The theoretical analysis of the TE and ED effects in semiconducting micromechanical structures consists in modeling a complex system by simultaneous analysis of the coupled plasma, thermal, and elastic wave equations.[23]

In the past years, techniques that drive the cantilever directly, such as magnetic modulation[24] and thermal modulation with resistive heating,[25] have been developed. The vibrations of the cantilever can be generated by a modulated laser photothermal (PT) process. Ratcliff *et al.*[26] reported that a PT excited cantilever has a well-defined single resonance mode while a cantilever mechanically driven by an external actuator generates an excitation spectrum showing many resonances especially in a solution. Kim and Lee[27] developed a technique to excite the self-oscillation of a metal-coated cantilever. Optical excitation is a noncontact technique and practically the same system can be used for excitation and detection.

Due to a wide use of semiconductor cantilevers in MEMS and the advantages of PT detection, the study of vibration spectra of microscale cantilevers under laser excitation aroused our research interests. There are few works on this topic. In this paper we study the vibration of millimeter-

[a)]Author to whom correspondence should be addressed. Electronic mail: bcretin@femto-st.fr.

 

sized semiconductor cantilevers induced by laser excitation using thermoelastic microscopy. It enabled one picometer resolution of photothermal signal amplitude in good adjustment conditions. The results showed that the experimental vibration spectra had a good agreement with the theoretical results. Also the slopes of PT signals were analyzed and showed that the amplitude and phase had a functional dependence on the modulation frequency.

## II. GENERAL THEORETICAL MODEL

### A. Plasma wave equation

Assuming that the energy of each photon, $E_e$, is greater than the semiconductor energy band gap $E_g$. Therefore, electrons are extracted from the valence band of the crystal to the conduction band, and electron-hole pairs are generated.

The time and space dependency of the plasma density $N$ is governed by the electron diffusion and by the nonradiative electron-hole recombination. Assuming Auger recombination is the dominant recombination mechanism, the corresponding diffusion equation is[22]

$$\frac{\partial N(\mathbf{r},t)}{\partial t} = D_E \nabla^2 N(\mathbf{r},t) - \frac{N(\mathbf{r},t) - N_0}{\tau} + \frac{Q(\mathbf{r},t)}{E_e}, \tag{1}$$

where $\mathbf{r}$ is the position vector, $t$ is the time variable, $D_E$ is the carrier diffusion coefficient, $\tau$ is the lifetime of photogenerated charge carriers, the so-called Auger recombination time, $N_0$ is the equilibrium carrier concentration, and $Q$ is the incident modulated laser source. In this paper we suppose lifetime is independent of the recombination probability.

Let us assume that the solution of the problem takes on following form:

$$N(\mathbf{r},t) = \bar{N}(\mathbf{r}) e^{j\omega t}, \tag{2}$$

where $\omega = 2\pi f$ is the modulation angular frequency. If the optical axis of the incident laser radiation is $z$ and the incident laser is irradiated at the surface of the sample, $Q$ can be given below as follows:

$$Q(x,y,z,\omega) = I_0(\omega)(1 - R_s)\frac{\alpha}{2E_e D_E} g(x,y) e^{-\alpha z}, \tag{3}$$

where the laser expansion according to the modulation frequency has been neglected. $I_0(\omega)$ is the incident energy, $R_s$ denotes the optical reflectance of the sample, and $\alpha$ is the optical absorption coefficient. $g(x,y)$ represents the distribution function of laser source at the surface of samples.

### B. Thermal wave equation

The temperature field $T(\mathbf{r},t)$ is governed by the following heat conduction equation:

$$\rho C_p \frac{\partial T(\mathbf{r},t)}{\partial t} = k\nabla^2 T(\mathbf{r},t) + \frac{E_g}{\tau}[N(\mathbf{r},t) - N_0] + \frac{(E_e - E_g)}{E_e} G(\mathbf{r},t), \tag{4}$$

where $\rho$ is the material density, $C_p$ stands for the specific heat, and $k$ is the thermal conductivity, and $G(\mathbf{r},t)$ is the carrier photogeneration source term. As shown in Ref. 28 three kinds of thermal source must be considered: (i) a fast thermal source, $G^T(z)$, due to the excess energy $\Delta E = E_e - E_g$ given off by the photogenerated carriers; (ii) a slow heat source, $G^{\mathrm{BR}}(z)$, which is contributed by the photogenerated carrier density and is transferred to the crystal lattice by the bulk recombination of the carriers; and (iii) heat sources, $G^{\mathrm{SR}}$, due to the carrier recombination at the surfaces of the semiconductor layer. So the periodic temperature field will be a sum of three components, the thermalization, bulk, and surface recombination components of the temperature distribution, and can be given below,

$$T(z) = T^T(z) + T^{\mathrm{BR}}(z) + T^{\mathrm{SR}}(z), \tag{5}$$

### C. Dynamic strain of the optically excited cantilever

Absorption of the optical energy in a semiconductor cantilever causes the various TE and ED effects. The TE and ED effects can be important as driven mechanisms for micromechanical structures, especially for cantilevers. The TE strain, $\varepsilon^{\mathrm{TE}}(\boldsymbol{r},t)$, that changes proportionally with temperature distribution, $T(\boldsymbol{r},t)$,

$$\varepsilon^{\mathrm{TE}}(\mathbf{r},t) = \alpha_T T(\mathbf{r},t), \tag{6}$$

where $\alpha_T$ is the coefficient of linear expansion. The electronic strain, $\varepsilon^{\mathrm{ED}}(\boldsymbol{r},t)$, changes linearly with excess carrier density, $N(\boldsymbol{r},t)$, and is given by

$$\varepsilon^{\mathrm{ED}}(\mathbf{r},t) = d_n N(\mathbf{r},t), \tag{7}$$

where $d_n$ is the coefficient of electronic elastic deformation. Since $d_n$ is negative for silicon, it means that the electronic strain and the thermal expansion are opposite in sign; the generation of excess carriers causes a contraction of the material, while thermal heating results in an expansion. The strain of cantilevers can be obtained as a sum of the TE and ED strains.

In the case of periodical excitation, with the angular modulating frequency of the incident laser excitation $\omega$, the dynamic equation for elastic bending of cantilever is[23]

$$\left[\frac{\partial^4}{\partial x^4} - k^4(\omega)\right] w(x,\omega) = 0, \tag{8}$$

where $k(\omega)$ is the wavenumber and

$$k^4(\omega) = \frac{\rho A}{B}\omega^2, \tag{9}$$

where $A$ is the cross-sectional area of the cantilever and $B = bh^3 E_Y / 12(1-\nu^2)$. The characteristic equation is expressed by

$$1 + \cos(\xi_n)\cosh(\xi_n) = 0, \quad \xi_n = k_n L, \quad (n = 1,2,\ldots). \tag{10}$$

The resonance frequency is

$$f_n = \frac{\xi_n^2}{4\pi}\frac{h}{L^2}\sqrt{\frac{E_Y}{3\rho(1-\nu^2)}}, \tag{11}$$

and $\xi_1 = 1.8751$ for first resonance frequency.

The displacement of the middle surface at the free end of the plate can be given as

$$w(L,\omega) = w_s(L,\omega)G(\omega), \tag{12}$$

where we have

$$w_s(L,\omega) = -\frac{L^2}{2}(\underline{m}_T + \underline{m}_n),$$

$$G(\omega) = \frac{2\sin\eta\sinh\eta}{\eta^2(1+\cos\eta\cosh\eta)},$$

$$\underline{m}_T = b\frac{\alpha_T m_T}{B}, \quad m_T = \int_0^h zT(x,z,t)dz,$$

$$\underline{m}_n = b\frac{d_n m_n}{B}, \quad m_n = \int_0^h zN(x,z,t)dz,$$

where $\eta = kL$, with $k^4(\omega) = \rho A\omega^2/B$.

Many authors theoretically studied the resonant frequency for cantilevers. For an oscillating rectangular cantilever in air the resonant frequency formulation were well documented in literature[29] by many authors as

$$f_n = \frac{1}{2\pi}\sqrt{\frac{K}{M_e}}, \tag{13}$$

where the parameter $K$ is the effective spring constant and depends on the thickness, density, and modulus of the cantilever material. $M_e$ is the effective mass of the cantilever.

## III. EXPERIMENTS

### A. Samples

Silicon cantilevers with different lengths and thicknesses have been fabricated in the clean room of FEMTO-ST using chemical etching process. The dimensions and characteristics of the Si cantilevers used in this paper were shown in Table I.

### B. Experimental setup

Figure 1 showed a block diagram of the experimental setup. This nondestructive apparatus mainly includes an optical probe (heterodyne interferometer with HeNe laser, $\lambda = 633$ nm). The details of optical probe are described in Refs. 15, 30, and 31. The excitation laser (doubled Nd doped yttrium aluminum garnet laser, $\lambda = 532$ nm) is modulated with an acousto-optic modulator (AOM), and the responses (the amplitude and phase) of the cantilever vibration are measured with a lock-in amplifier (the detection range is 1–120 kHz). This setup was installed on an antivibration table. A wave generator was used to modulate the excitation laser. Due to the interference of probe laser beam and the reflected one, the small vibration of the samples induced by the heating of excitation laser could be recorded as the resulting PT signals. These signals have been sent to lock-in amplifiers in order to extract the magnitude and phase of the displacement for each modulation frequency. The intensity of excitation laser beam was 200 mW and the one of probe

TABLE I. The dimensions and characteristics of the Si cantilevers were used in this work.

| No. of cantilever | Length ($\mu$m) | Width ($\mu$m) | Thickness ($\mu$m) | Material resistivity Si ($n$-type) ($\Omega$ cm) | Mass (kg) |
|---|---|---|---|---|---|
| 1 | 1498 | 389 | 138 | 3–7 | $1.87\times10^{-7}$ |
| 2 | 1495 | 366 | 64 | 3–7 | $8.15\times10^{-8}$ |
| 3 | 2001 | 385 | 155 | 3–7 | $2.78\times10^{-7}$ |
| 4 | 2008 | 369 | 81 | 3–7 | $1.40\times10^{-7}$ |
| 5 | 2001 | 392 | 150 | 3–7 | $2.74\times10^{-7}$ |
| 6 | 2507 | 392 | 159 | 3–7 | $3.64\times10^{-7}$ |
| 7 | 3003 | 398 | 158 | 3–7 | $4.4\times10^{-7}$ |

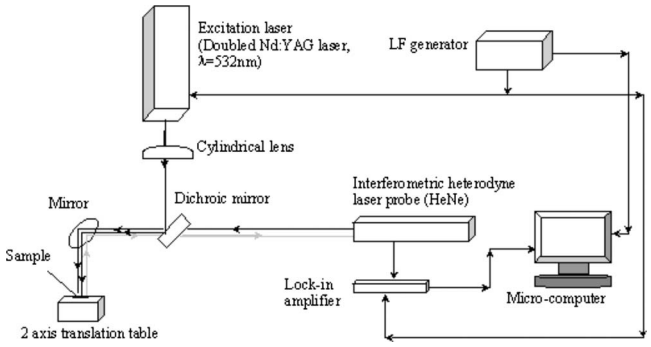


FIG. 1. Experimental apparatus of the thermoelastic microscope.

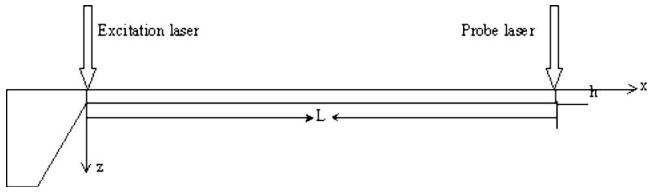


FIG. 2. Rectangular cantilever with laser excitation and probe.

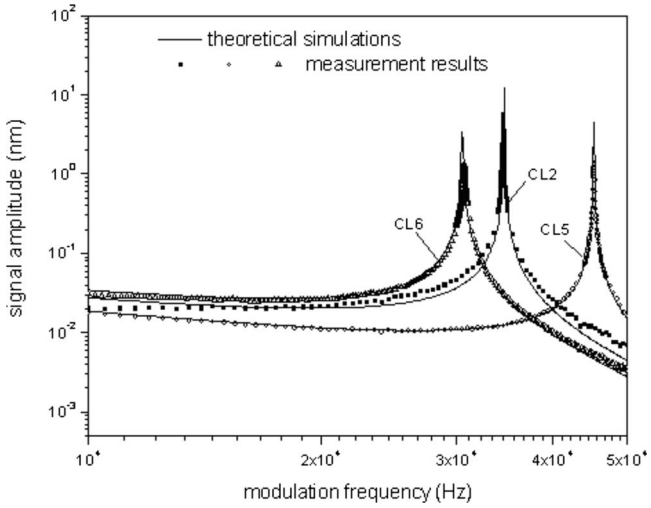


FIG. 3. Theoretical and experimental amplitude of the vibration generated at the free end of the cantilevers.

TABLE II. The comparison of experimental and theoretical resonance frequencies for different cantilevers.

| | Resonance frequency (kHz) | | | | | |
|---|---|---|---|---|---|---|
| | | Theor. | | | | |
| No. of cantilever | Expt. | Reference 29 | Relative error (%) | Our results | Relative error (%) | $Q$ factor |
| 1 | 70.2 | 73.4 | 4.7 | 74.5 | 6.1 | 44 |
| 2 | 34.5 | 34.2 | 0.9 | 34.7 | 0.6 | 492 |
| 3 | 47.7 | 46.2 | 3.1 | 46.9 | 1.7 | 136 |
| 4 | 24.2 | 24.0 | 0.8 | 24.3 | 0.4 | 404 |
| 5 | 45.3 | 44.7 | 1.3 | 45.4 | 0.2 | 452 |
| 6 | 30.7 | 30.2 | 1.6 | 30.6 | 0.3 | 139 |
| 7 | 21.6 | 21.7 | 4.6 | 21.6 | 0.1 | 115 |

beam was 3 mW. The two laser beams were unfocused. The samples were glued on plastic holders and put on the two axis translation table.

The position of the excitation beam on the cantilever can be accurately adjusted with this table to obtain the maximum vibration signal. Figure 2 describes the position of the two beams and the configuration of cantilevers. The measurement results used in this paper are the mean values of at least three measurements at the same excitation and detection position. The results have showed that the measurement has a good reproducibility.

## IV. RESULTS AND DISCUSSION

### A. Resonance frequency

Using the interferometer setup described above, we measured some cantilevers of different sizes. To obtain the uniform excitation at the surface of cantilevers, a cylindrical lens was used between the excitation laser and the dichroic mirror. The resonance frequency of the experiments and simulations are shown in Table II. Near the resonance frequency the measurement was carried out with small frequency steps (100 Hz). It can be seen from this table that the resonance frequencies obtained by experiments agree well with that of simulations. The relative errors are below 6%. For the short cantilevers (Nos. 1 and 2), the difference between theoretical and experimental data showed that the three dimensional (3D) contributions to the structure could not be neglected. In the calculation below, the following parameters were used for silicon: thermal expansion: $\alpha_T=3\times10^{-6}$ 1/K, coefficient of electronic deformation: $d_n=-9\times10^{-31}$ m$^3$, reflectance of the sample surface: $R_s=0.3$, excitation energy: $E=1.96$ eV, energy gap: $E_G=1.11$ eV, $\Delta E=(E-E_G)=0.85$ eV, coefficient of carrier diffusion: $D_E=2.5\times10^{-3}$ m$^2$/s, coefficient of optical absorption: $\alpha=5\times10^5$ m$^{-1}$, lifetime of photogenerated carriers: $\tau=5\times10^{-5}$ s, surface recombination velocities on the front (optically excited) side: $s_g=2$ m/s, on the back side: $s_b=3$ m/s, $\gamma_G=\gamma_R=1.0$, thermal conductivity: $K=150$ W/(m K), thermal diffusivity: $D_T=K/(\rho C)=0.926\times10^{-4}$ m$^2$/s, density: $\rho=2.33\times10^3$ kg/m$^3$, the thermal capacity: $C=695$ J/(kg K), Young's modulus: $E_Y=1.31\times10^{11}$ N/m$^2$, and Poisson's ratio: $\nu=0.2$; for air the following parameters were used: thermal conductivity: $K=0.025$ W/(m K), thermal diffusivity: $D_T=0.0206$ m$^2$/s, density: $\rho=1.205$ kg/m$^3$, and the thermal capacity: $C_2=1.013\times10^3$ J/(kg K).

### B. Vibration spectra for different sized cantilevers

Figures 3 and 4 showed the results of experimental and theoretical estimations for amplitude and phase of cantilever Nos. 2, 5, and 6. In these measurements the pump laser heating sources were uniform at the whole surface of cantilevers and probe lasers at the free end. Each experiment was repeated at least three times and the resonance frequencies were stable in the different measurements. This denoted that the mechanical properties of the cantilever were stable. The two figures showed a typical frequency dependence of the PT signal. Due to high detection frequency and relatively high excitation power the experiment results showed that the background noise and vibration of the environment around had almost no influence on our measurements. Also the resonance spectra of PT amplitude signals showed that this setup could give stable picometric vibration signal.

We can see for the signal amplitude that the theoretical and experimental results had a good agreement in the frequency domain of 10–50 kHz (near resonant frequency) for 2 and 2.5 mm length cantilevers (CL5 and CL6).

For 1.5 mm length cantilever (CL2) the difference between the theoretical and measurement results could not be

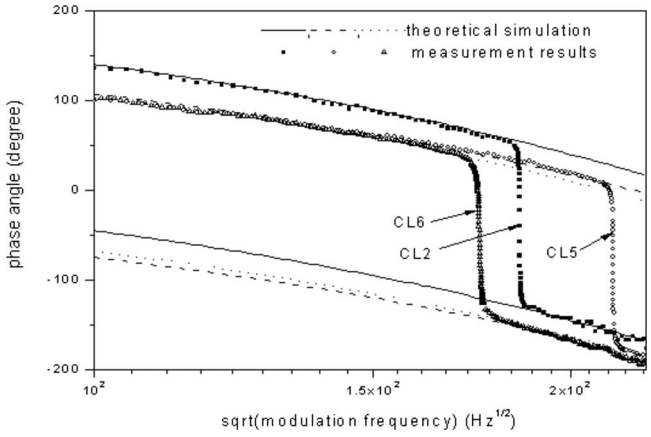


FIG. 4. Theoretical and experimental phase of the vibrations with square root of modulation frequency.

TABLE III. The slopes of amplitude and phase for 2.5 mm cantilever under different excitation positions.

| | Amplitude | | | Phase | | |
|---|---|---|---|---|---|---|
| Position of excitation probe | Range of modulation frequency (kHz) | Power $\alpha$ $(A \propto \omega_m^{-\alpha})$ | Relative error of the power $\alpha$ (%) | Range of modulation frequency (kHz) | Slope $\beta$ $(\phi \propto \beta\omega_m^{1/2})$ | Relative error of the slope (%) |
| Free-free | 10–25 | −0.636 | 2.7 | 10–44 | −0.912 | 0.9 |
| Mid-free | 10–25 | −0.611 | 0.5 | 10–44 | −0.873 | 0.5 |
| Mid-mid | 10–25 | −0.472 | 2.6 | 10–44 | −0.906 | 0.4 |
| Clamp-free | 10–25 | −0.623 | 1.3 | 10–44 | −0.864 | 0.4 |
| Clamp-mid | 10–25 | −0.620 | 1. 3 | 10–44 | −0.868 | 0.4 |
| Clamp-clamp | 10–25 | −0.508 | 3.1 | 10–44 | −0.924 | 0.6 |

neglected. The reason can be understood with the increase in length-to-width ratio of the cantilever: the three dimensional contributions will be dominant. A more precise 3D mathematical model should be used to simulate the problem. We also observed that the measurement amplitudes at resonance are below than that of theoretical ones. This is mainly because of energy losses and vibration damping in practical cases.

For the phase angle the agreement was acceptable at relatively low modulation frequency (below 25 kHz). But at a relatively high modulation frequency (above 25 kHz) there was unnegligible deviation between them. Whatever the theoretical simulation or experimental measurement, we noted that the resonant peaks were followed by a sharp change of 180° for phase angle as expected.

### C. Slopes of the PT signal amplitude and phase angle under different excitation and detection positions

We measured two silicon cantilevers under different excitation and detection positions. In these measurements the excitation laser sources were focused using a microscope objective (20×). The measurement results were analyzed for signal curve slopes in a certain modulation frequency domain and showed in Tables III and IV. The results revealed that the signal amplitude changes as a power function of modulation frequency $\omega_m$, i.e., $A \propto \omega_m^{-\alpha}$. The parameter $\alpha$ depended on the properties of the samples and the detection position. The phase angle has a linear dependence on the square root of modulation frequency $\omega_m^{1/2}$, i.e., $\phi \propto \beta\omega_m^{1/2}$. Also from Tables III and IV we could notice that for different samples the slopes of phase were almost the same (small difference below 3.5%). This means phase angles were independent of the laser source and sample size and only as a function of material properties. The same phenomenon could also be observed in Fig. 3. This conclusion was the same as that obtained by Pelzl and Netzelmann.[13]

## V. CONCLUSION

The vibrations of rectangular silicon cantilevers, induced by laser excitation, were measured using thermoelastic microscopy under different modulation frequencies. The small response signal can be obtained (the measured vibration amplitude can below ten picometer in good adjustment) at a high modulation frequency. The results show that the signal amplitudes correspond to a power function of the modulation frequency and that the phase angle changed linearly with the square root of the modulation frequency. The experimental results agreed well with theoretical ones.

## ACKNOWLEGMENTS

Yaqin Song gratefully thanks the support of La Fondation Franco-Chinoise Pour la Science et ses Application (FFCSA) and National Natural Science Foundation of China (Grant No. 10502041).

TABLE IV. The slopes of amplitude and phase for 3 mm cantilever under different excitation positions.

| | Amplitude | | | Phase | | |
|---|---|---|---|---|---|---|
| Position of excitation-probe | Range of modulation frequency (kHz) | Power $\alpha$ $(A \propto \omega_m^{-\alpha})$ | Relative error of the power $\alpha$ (%) | Range of modulation frequency (kHz) | Slope $\beta$ $(\phi \propto \beta\omega_m^{1/2})$ | Relative error of the slope (%) |
| Free-free | 2–15 | −0.483 | 3.2 | 7–20 | −0.925 | 1.2 |
| Mid-free | 2–15 | −0.398 | 2.8 | 7–20 | −0.882 | 0.8 |
| Mid-mid | 4–10 | −0.280 | 8.3 | 7–20 | −0.902 | 1.4 |
| Clamp-free | 2–15 | −0.323 | 5.5 | 7–20 | −0.882 | 0.9 |
| Clamp-mid | 2–15 | −0.326 | 4.6 | 7–20 | −0.880 | 0.8 |
| Clamp-clamp | 4–13 | −0.318 | 5.5 | 7–20 | −0.929 | 1.0 |

[1]A. M. Korsunsky, S. Cherian, R. Raiteri, and R. Berger, Sens. Actuators, A **139**, 70 (2007).
[2]K. Rijal and R. Mutharasan, Sens. Actuators B **124**, 237 (2007).
[3]D. Maraldo and R. Mutharasan, Sens. Actuators B **123**, 474 (2007).
[4]G. A. Campbell and R. Mutharasan, Biosens. Bioelectron. **21**, 1684 (2006).
[5]G. A. Campbell, M. B. Medina, and R. Mutharasan, Sens. Actuators B **126**, 354 (2007).
[6]A. Mandelis, *Photoacoustic and Thermal Wave Phenomena in Semiconductors* (North-Holland, New York, 1987), p. 145.
[7]H. Vargas and L. C. M. Miranda, Phys. Rep. **161**, 43 (1988).
[8]P. M. Nikolić and D. M. Todorović, Prog. Quantum Electron. **13**, 107 (1989).
[9]D. Almond and P. Patel, *Photothermal Science and Techniques* (Chapman and Hall, London, 1996), p. 138.
[10]A. Mandelis and K. H. Michaelian, Opt. Eng. (Bellingham) **36**, 301 (1997).
[11]A. Mandelis and P. Hess, *Progress in Photothermal and Photoacoustic Science and Technology* (SPIE, Bellingham, Washington, 2000), p. 147.
[12]G. E. Sandoval-Romero, A. Garcia-Valenzuela, C. Sanchez Perez, J. Hemandez-Cordero, and K. L. Muratikov, Rev. Sci. Instrum. **78**, 104901 (2007).
[13]*Topics of Current Physics*, edited by P. Hess (Springer-Verlag, Berlin, 1989), p. 129.
[14]B. Cretin, N. Daher, and B. Cavallier, Proc. SPIE **3098**, 466 (1997).
[15]B. Cretin and P. Vairac, Appl. Phys. A: Mater. Sci. Process. **66**, S235 (1998).
[16]J. Jumel, D. Rochais, and F. Enguehard, Rev. Sci. Instrum. **74**, 608 (2003).
[17]T. Ikari, J. P. Roger, and D. Fournier, Rev. Sci. Instrum. **74**, 553 (2003).
[18]J. Jumel, F. Lepoutre, D. Rochais, and F. Enguehard, Rev. Sci. Instrum. **74**, 540 (2003).
[19]D. Dietzel, B. K. Bein, and J. Pelzl, J. Appl. Phys. **93**, 9043 (2003).
[20]C. J. Stolz, D. J. Chinn, R. D. Huber, C. L. Weinzapfel, and Z. Wu, Proc. SPIE **5273**, 373 (2004).
[21]T. Ikari, A. Fukuyama, T. Murata, M. Suemitsu, N. Haddad, B. Reita, J. P. Roger, and D. Fournier, Mater. Sci. Eng., B **124–125**, 345 (2005).
[22]D. M. Todorović, Rev. Sci. Instrum. **74**, 582 (2003).
[23]D. M. Todorović, Rev. Sci. Instrum. **74**, 578 (2003).
[24]W. Han, S. M. Lindsay, and T. Jing, Appl. Phys. Lett. **69**, 4111 (1996).
[25]A. C. Hillier and A. J. Bard, Rev. Sci. Instrum. **68**, 2082 (1997).
[26]G. C. Ratcliff, D. A. Erie, and R. Superfine, Appl. Phys. Lett. **72**, 1911 (1998).
[27]K. Kim and S. Lee, J. Appl. Phys. **91**, 4715 (2002).
[28]D. M. Todorović, P. M. Nikolić, and A. I. Bojičić, J. Appl. Phys. **85**, 7716 (1999).
[29]G. Y. Chen, T. Thundat, E. A. Wachter, and R. J. Warmack, J. Appl. Phys. **77**, 3618 (1995).
[30]P. Vairac and B. Cretin, Opt. Commun. **132**, 19 (1996).
[31]B. Cretin and P. Vairac, Appl. Phys. A: Mater. Sci. Process. **A66**, s235 (1998).